Macromolecules

Article

pubs.acs.org/Macromolecules

Dynamics of Unentangled *cis*-1,4-Polyisoprene Confined to Nanoporous Alumina

Stelios Alexandris,[†] Georgios Sakellariou,[‡] Martin Steinhart,[§] and George Floudas*[,†]

[†]Department of Physics, University of Ioannina, 45110 Ioannina, Greece

[‡]Department of Chemistry, University of Athens, 15771 Athens, Greece

[§]Institut für Chemie neuer Materialien, Universität Osnabrück, D-49069 Osnabrück, Germany

Supporting Information

ABSTRACT: The dynamics of unentangled *cis*-1,4-polyisoprene confined within self-ordered nanoporous alumina (AAO) is studied as a function of molecular weight (5000−300 g/mol) and pore size (400−25 nm) with dielectric spectroscopy. The main effects are the pronounced broadening of both segmental and chain modes with decreasing AAO pore diameter. This suggests that the global chain relaxation is retarded on confinement. Remarkably, the distribution of relaxation times is broadened even within pores with size 50 times the unperturbed chain dimensions. The glass temperature is unaffected by confinement. These results are discussed in terms of confinement and adsorption effects. Confinement effects are negligible for the studied molecular weights. Chain adsorption, on the other hand, involves time and length scales distinctly different from the bulk that can account for the experimental findings.

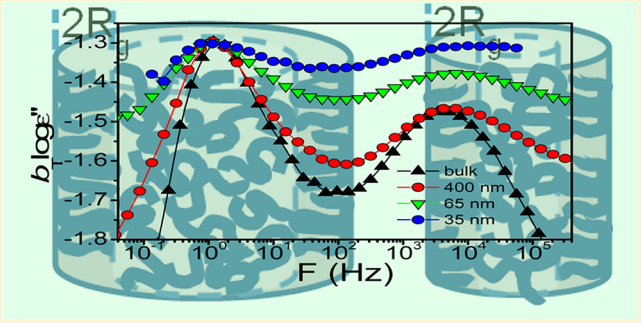

I. INTRODUCTION

Confined liquids found for example in a cell membrane or in contact with solid surfaces and within porous media show structural and dynamic features distinctly different from the bulk.[1] Likewise, confined polymers can exhibit structural and dynamic properties that can be different from the bulk. Chain conformation, chain interpenetration, and eventually flow may be influenced by confinement.[2,3] Polymer−wall and polymer−substrate interactions can give rise to adsorption and to the formation of different configurations (trains, loops, tails) that will affect both the structural and dynamic properties.[4−10] These effects need to be considered as they will have profound implications in the design and processing of polymeric nanostructured devices.

Earlier works studied the effect of confinement on the dynamics of type A polymers including *cis*-1,4-polyisoprene (PI).[11−17] Type A polymers are advantageous for such studies because of the nonzero components of the dipole moment perpendicular and parallel to the chain contour giving rise to the respective "fast" segmental and "slow" global chain (also called normal) modes. In these studies the confining medium varied from controlled porous glasses[6,11,18]—with a rather broad pore size distribution—to thin polymer films[11−15,17] that were deposited on different substrates (mica, silica) and even having a free interface.[17] Because of the different polymer/substrate interactions, it is difficult to put all results in perspective. However, there is consensus that for PIs bearing molecular weights below the entanglement molecular weight ($M_e \sim 5000$ g/mol) there is a broadening of the segmental and chain mode dynamics under confinement. For higher molecular weights a new mode is reported at frequencies intermediate to the bulk segmental and normal mode processes. The latter mode is attributed to the dynamic adsorption/desorption process of chain segments that resulted in a faster subchain relaxation of suppressed intensity.[11,13,17]

Self-ordered nanoporous aluminum oxide (AAO)[19−22] contains arrays of parallel, cylindrical nanopores that can be employed as model system in studying the effect of confinement on polymer structure and dynamics. Recent studies of amorphous polymers within AAO explored the chain conformation[2,3,8] and chain mobility[2,9] issues. However, it is unknown how the uniform 2D-confinement and nature of pore walls affects the dynamics of a typical type A polymer like *cis*-1,4-polysiprene (PI).

Here we explore the effect of 2D-confinement on the segmental and chain dynamics of a series of unentangled PIs. We find that 2D-confinement does not alter significantly the local segmental dynamics. It is astonishing to see that the distribution of relaxation times for both modes is broadened even within pores with size 50 times the unperturbed chain dimensions. This is discussed in terms of confinement and adsorption effects with the latter exerting the major influence.

Received: April 1, 2014
Revised: June 5, 2014
Published: June 11, 2014

ACS Publications © 2014 American Chemical Society

dx.doi.org/10.1021/ma5006638 | *Macromolecules* 2014, 47, 3895−3900

Table 1. Molecular Characteristics, VFT Parameters for the Segmental and Global Chain Relaxation Modes, and DSC and DS Glass Temperatures of *cis*-1,4-Polyisoprenes in the Bulk Employed in This Study

			segmental mode			normal mode				
code	M_n (g/mol)	M_w (g/mol)	τ_0 (s)	B (K)	T_0 (K)	τ_0 (s)	B (K)	$T_0{}^a$ (K)	$T_g{}^b$ (K) (DSC)	$T_g{}^c$ (K) (DS)
I_4	300		2×10^{-12}	1300 ± 150	134 ± 3	5×10^{-11}	1220 ± 20	134	178	175
I_7	500	560	5×10^{-12}	1400 ± 120	138 ± 3	6×10^{-11}	1250 ± 20	138	182	180
I_{12}	800	880	1×10^{-13}	1500 ± 120	146 ± 2	1×10^{-10}	1290 ± 10	146	191	189
I_{24}	1600	1730	9×10^{-11}	1220 ± 70	160 ± 2	9×10^{-11}	1140 ± 10	160	197	198
I_{74}	5000	5250	2×10^{-12}	1410 ± 50	163 ± 1	9×10^{-9}	1320 ± 10	163	209	205
I_{294}	2×10^4	2.08×10^4	4×10^{-12}	1410 ± 60	166 ± 1	4×10^{-7}	1310 ± 10	166	211	208
I_{1470}	1×10^5	1.06×10^5	7×10^{-13}	1290 ± 20	168 ± 1					208

[a]Held fixed to the corresponding value from the segmental mode. [b]Cooling rate 10 K/min. [c]At τ = 100 s.

II. EXPERIMENTAL SECTION

Samples and Method of Infiltration. PI samples with different molecular weights (Table 1) were synthesized via anionic polymerization following standard procedures.[23] Self-ordered AAO (pore diameters of 25, 35, 65, 200, and 400 nm; pore depth 100 μm) was prepared following the procedures reported in the literature.[19−21]

The microstructure was 93% 1,4 and 7% 3,4 units. An Al with a thickness of about 1 mm at the bottom of templates served as the lower electrode. Before infiltration the AAO templates were placed in an oven under vacuum at a temperature of 170 °C for 8−10 h. Infiltration of PIs was performed at inert atmosphere conditions (argon) within a glovebox by placing a drop (about 10 mg) on top of the self-ordered AAO at 20 °C for 24 h. Following infiltration the top surface was carefully cleaned using absorbing paper and a small amount of toluene. Two ways were employed herein to obtain the PI volume fraction. First, templates were weighted before and after infiltration. Second, AAO porosity was estimated by digitizing SEM images (SEM images were obtained at acceleration voltages from 0.75 to 6 kV with in-lense secondary electron detectors, which are most suitable for this type of analysis) of empty self-ordered AAO. The latter resulted in PI volume fractions (100% filling) of 0.58 (400 nm), 0.26 (200 nm), 0.44 (65 nm), 0.14 (35 nm), and 0.40 (25 nm). The two methods were in good agreement. Contact angle measurements on treated and untreated Al_2O_3 surfaces were made at ambient temperature, and the results are included in the Supporting Information. These measurements revealed that PI wets the Al_2O_3 surface, which is suggestive of attractive interactions. High temperature annealing might reduce the number of hydroxyl groups. This may lead to reduction in the dominant polar surface energy and in an increase in the dissipative surface energy. In the DS study below we used thermally treated templates.

Scanning Electron Microscopy. Scanning electron microscopy (SEM) investigations using a LEO Gemini 1530 SEM, operated at acceleration voltages from 0.75 to 6 kV, revealed complete filling of pores. Figure 1 gives SEM images of I_{74} infiltrated in self-ordered AAO with different pore diameters.

Differential Scanning Calorimetry. Differential scanning calorimetry (DSC) measurements were made with a Q2000 (TA Instruments) with a cooling/heating rate of 10 K/min. The obtained glass temperatures are included in Table 1.

Dielectric Spectroscopy. Dielectric spectroscopy (DS) measurements were performed at different temperatures in the range of 143−313 K, at atmospheric pressure, and for frequencies in the range from 10^{-2}−10^7 Hz. Measurements were made with a Novocontrol Alpha frequency analyzer composed of a broadband dielectric converter and an active sample hand. For bulk PIs, the DS measurements were carried out in the usual parallel plate geometry with electrodes of 20 mm in diameter and a sample thickness of 50 μm maintained by Teflon spacers. For the PI infiltrated self-ordered AAO samples, a 10 mm electrode was placed on the AAO surface. In all cases, the complex dielectric permittivity $\varepsilon^* = \varepsilon' - i\varepsilon''$, where ε' is the real and ε'' is the imaginary part, was obtained as a function of frequency ω and temperature T, i.e., $\varepsilon^*(T, \omega)$.[24−26] The measured dielectric spectra were corrected for the geometry by using two capacitors in parallel

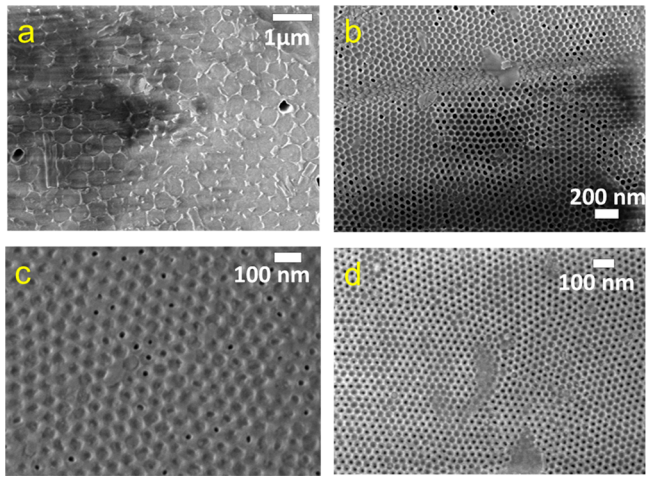

Figure 1. Scanning electron microscopy images of I_{74} infiltrated in self-ordered AAO: (a) pore diameter of 400 nm, (b) pore diameter of 65 nm, (c) pore diameter of 35 nm, and (d) with pore diameter of 25 nm. The white scale bars are shown.

(composed of ε^*_{PI} and ε^*_{AAO} and the measured total impedance was related to the individual values through $1/Z^* = 1/Z^*_{PI} + 1/Z^*_{AAO}$).[27] A comparison of dielectric spectra of empty and filled pores is included in the Supporting Information. This allows calculating the real and imaginary parts of the dielectric permittivity as a function of the respective volume fractions. The analysis was done using the empirical equation of Havriliak and Negami (HN):[28]

$$\varepsilon^*_{HN}(\omega, T) = \varepsilon_\infty(T) + \frac{\Delta\varepsilon(T)}{[1 + (i\omega\tau_{HN}(T)^m)]^n} + \frac{\sigma_0(T)}{i\varepsilon_f\omega} \quad (1)$$

Here, $\Delta\varepsilon(T)$ is the relaxation strength of the process under investigation, τ_{HN} is the relaxation time of the equation, and m, n ($0 < m, mn \leq 1$) describe the symmetrical and asymmetrical broadening of the distribution of relaxation times and ε_∞ is the dielectric permittivity at the limit of high frequencies. Although the spectral shape of the segmental mode can well be described by the HN function, the shape of the chain dynamics—that includes a collection of modes with different amplitudes and relaxation times—cannot be described by a single HN function.[26] However, because of the low molecular weights employed herein, there is significant spectral overlap between the segmental and chain modes and a summation of two HN functions suffice to describe the dielectric response under confinement. The relaxation times at maximum loss (τ_{max}) are presented herein and have been analytically obtained by the Havriliak−Negami equation as follows:

$$\tau_{max} = \tau_{HN} \sin^{-1/m}\left(\frac{\pi m}{2(1+n)}\right) \sin^{1/m}\left(\frac{\pi mn}{2(1+n)}\right) \quad (2)$$

dx.doi.org/10.1021/ma5006638 | Macromolecules 2014, 47, 3895−3900

These relaxation times correspond to the global chain relaxation in the bulk and to the relaxation of the most intense chain mode (which is not necessarily the global chain relaxation) under confinement. At lower frequencies, ε'' rises due to the conductivity ($\varepsilon'' = \sigma/(\omega\varepsilon_f)$, where σ is the dc conductivity and ε_f the permittivity of free space). The conductivity contribution has also been taken into account during the fitting process.

III. RESULTS AND DISCUSSION

Bulk PI Dynamics. The dynamics of type A polymers including PIs have been well studied in the past as a function of molecular weight,[29−35] temperature, and pressure,[36,37] and the successes and weaknesses of the Rouse model have been discussed in detail.[38−41] Here we briefly mention the bulk dynamics of the studied PIs. In all cases, the shape of the global chain dynamics has the typical terminal behavior with a low frequency slope, $m = 1$ (i.e., $\varepsilon'' \sim \omega$). The temperature dependence of the relaxation times corresponding to the bulk PIs are shown in Figure 2. The figure depicts the segmental and

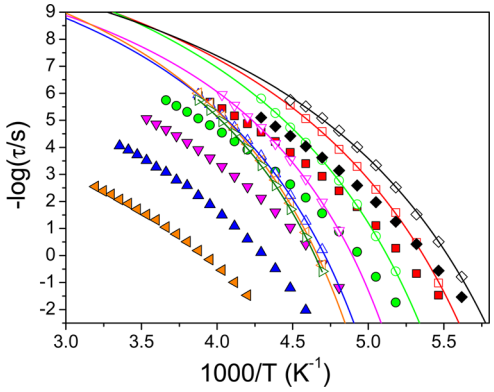

Figure 2. Relaxation map for the bulk PIs with the segmental processes (open symbols) and global chain relaxation (filled symbols); (rhombi): I_4, (squares): I_7, (circles): I_{12}, (down triangles): I_{24}, (up triangles): I_{74}, (left triangles): I_{294} and (right triangles): I_{1470}. Solid lines represent fits to the VFT equation for the segmental processes only for clarity.

longest Rouse (i.e., terminal) relaxation times that both conform to the usual Vogel−Fulcher−Tammann (VFT) equation:

$$\tau = \tau_0 \exp\left(\frac{B}{T - T_0}\right) \quad (3)$$

where τ_0 is the relaxation time in the limit of very high temperatures, B is the activation parameter, and T_0 is the "ideal" glass temperature. These parameters for both processes are summarized in Table 1 together with the DSC glass temperature, T_g (rate 10 K/min).

The glass temperature, as obtained from the VFT fits to the segmental process (at $\tau = 10^2$ s), is plotted in Figure 3 as a function of molecular weight. The dependence conforms to the Fox−Flory equation $T_g(M_w) = T_g^\infty - A/M_w$, where T_g^∞ (= 208 K) is the glass temperature in the limit of very high molecular weight and A (= 11600 ± 900 g K/mol) is a fitting parameter. In the inset to Figure 3, the relaxation times corresponding to the global chain relaxation peak is plotted as a function of molecular weight. Because of the strong molecular weight dependence of the segmental process, the characteristic times of the global chain mode is normalized to the respective

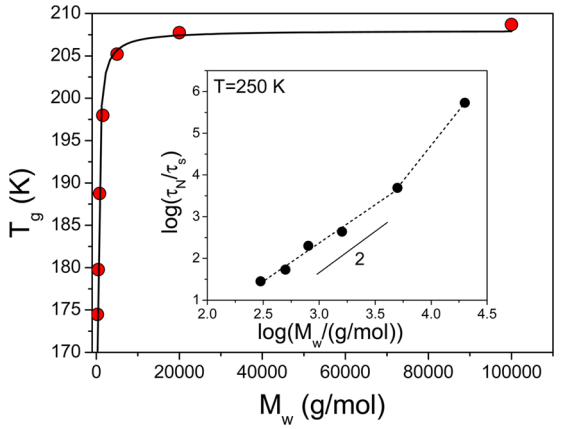

Figure 3. Molecular weight dependence of the glass temperatures of bulk PIs. The line is a fit to the Fox−Flory equation (see text). In the inset, the longest normal mode times normalized by the corresponding segmental times are plotted as a function of molecular weight in a double-logarithmic representation. A line with a slope of 2 is shown signifying the Rouse regime. Only PI's within the Rouse regime were investigated in this study.

segmental times. The obtained linear dependence with a slope of ∼2 in the log−log representation confirms that samples I_4, I_7, I_{12}, I_{24}, and I_{74} all belong to the Rouse regime, in agreement with the reported value for the molecular weight between entanglements ($M_e \sim 5000$ g/mol).[42]

PI Dynamics within Self-Ordered AAOs. Figure 4 compares dielectric loss spectra of bulk I_{74} with spectra from

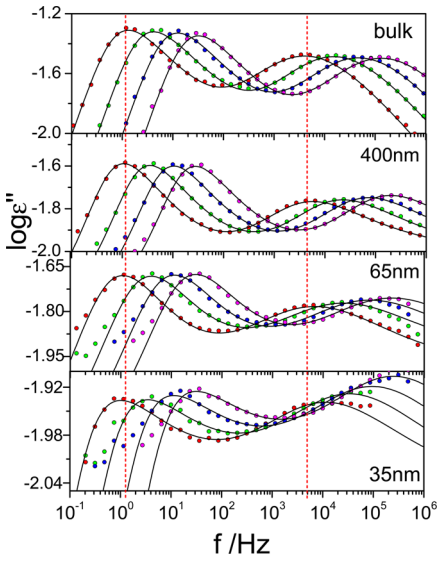

Figure 4. Dielectric loss spectra of bulk I_{74} and of I_{74} located inside self-ordered AAO with pore diameters of 400, 65, and 35 nm at four temperatures: (red spheres) 233 K; (green spheres) 238 K; (blue spheres) 243 K; (magenta spheres) 248 K. Vertical lines give the approximate positions of the segmental and longest normal mode for the bulk PI.

the same polymer located inside self-ordered AAO at four selected temperatures. The "fast" and "slow" processes correspond to the segmental and chain modes, respectively. The two vertical lines indicate the peak positions of the two processes in the bulk I_{74}. It can be seen that under confinement both processes are approximately at the same position as in the

dx.doi.org/10.1021/ma5006638 | Macromolecules 2014, 47, 3895−3900

bulk. This does not necessarily mean that global chain dynamics are identical in bulk and under confinement.[39] In bulk, a true terminal relaxation is obtained (m = 1) whereas under confinement the low frequency slope remains solely below 1. Hence, the global chain dynamics of PI inside self-ordered AAO is retarded and the degree of retardation depends on pore size. To facilitate a comparison with the bulk, here we employ the most intense chain mode. The comparison is shown in the Arrhenius representation of relaxation times in Figure 5. The figure compares the segmental and most intense

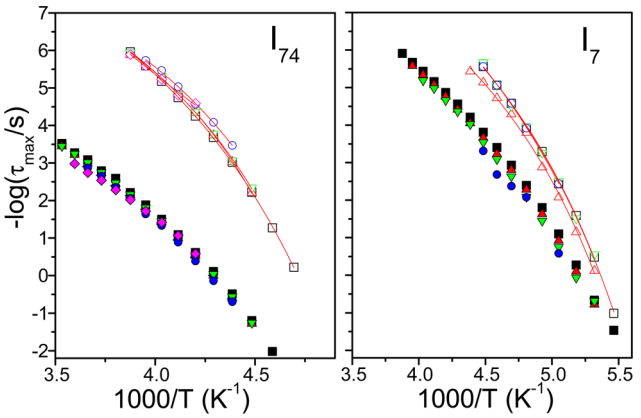

Figure 5. Arrhenius relaxation map for the segmental (open symbols) and most intense chain mode (filled symbols) processes of bulk I_7 and I_{74} (square symbols) as well as for the I_7 and I_{74} located inside self-ordered AAO with pore diameters of 400 nm (up triangles), 100 nm (left triangles), 65 nm (down triangles), 35 nm (circles), and 25 nm (rhombi). The uncertainty of relation times is smaller than the symbol size in I_{74} and approximately the symbol size in I_7.

chain mode relaxation times for two PIs: I_7 and I_{74}. For the I_{74} located inside self-ordered AAO, the segmental and most intense chain dynamics are nearly indistinguishable from the bulk. However, for I_7 located inside self-ordered AAO there is weak dependence of the chain process on confinement.

Interestingly, the higher the confinement, the slower the chain dynamics is. In addition, a slight speed-up of the segmental mode in the smaller pores (35 and 25 nm) can be seen which is beyond the experimental uncertainty (smaller than the symbol size in I_{74} and approximately the symbol size in I_7).

Remarkably, the distribution of relaxation times for both processes is strongly affected by confinement. This is depicted in Figure 6 where the dielectric loss spectra for bulk I_{74} and I_{74} located inside self-ordered AAO with different pore diameters are compared at the same temperature. It can be readily seen that the main effect of confinement is to broaden both the segmental and chain modes. This effect exists even for PIs located inside self-ordered AAO with the larger pore diameter (400 nm). Despite this, one should note a different (smaller) high frequency slope ($-mn$) for the segmental mode. This high frequency slope has been discussed as reflecting local chain dynamics that are affected by chain adsorption on the alumina walls.[43] This effect becomes very pronounced in the smaller pores; from a bulk value of $n \sim 0.5$ to $n \sim 0.2$ for I_{74} within self-ordered AAO with a pore diameter of 25 nm. The variation of the distribution parameter m for the segmental and chain modes of the different PIs within self-ordered AAO with pore diameters in the range from 400 to 25 nm is shown in Figure 7. The figure depicts pronounced broadening of both the modes

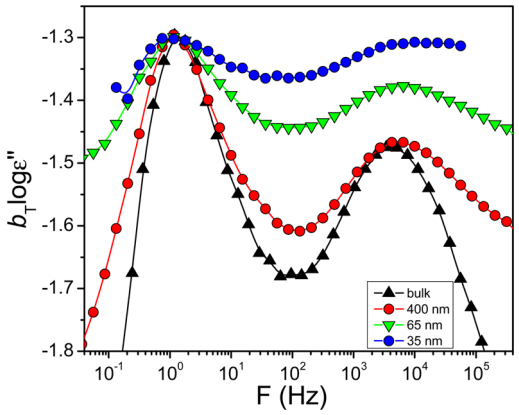

Figure 6. Comparison of the dielectric loss data for bulk I_{74} and for I_{74} located inside self-ordered AAO with pore diameters of 400, 65, and 35 nm at 233 K. The data have been vertically shifted (vertical shift factor b_T) so as to coincide at the maximum of the dielectric loss peak corresponding to the most intense chain mode but not horizontally.

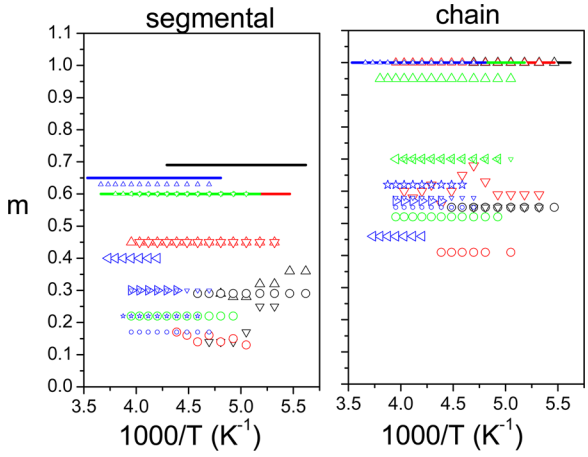

Figure 7. Low frequency slope, m, corresponding to the segmental (left) and chain modes (right) for different PIs in the bulk (lines) and for PIs located within self-ordered AAO: (black symbols) I_4, (red symbols) I_7, (green symbols) I_{12}, and (blue symbols) I_{23}. The pore diameters are (up triangles) 400 nm, (right triangles) 200 nm, (left triangles) 100 nm, (down triangles) 65 nm, (circles) 35 nm, and (stars) 25 nm.

within self-ordered AAO. This again suggests that a true terminal relaxation has not been reached under confinement and that the true global chain relaxation is retarded. Furthermore, the smaller the pores, the stronger the retardation is.

These findings can be discussed in terms of confinement and adsorption effects. In general, confinement can affect molecular dynamics. Under confinement the number of available configurations of a polymer chain is reduced. This leads to a free energy excess that for an ideal chain with size $R = aN^{1/2}$, where N is the number of monomers and a is the monomer size, trapped in a tube of characteristic size D is[44]

$$\frac{F_{conf}}{k_B T} \cong \left(\frac{R}{D}\right)^2 \quad (4)$$

At this point we do not invoke any attraction to the pore walls. Equation 4 results from the reduced entropy under confinement with ΔS being (i) a linear function of N (extensive variable) and (ii) dimensionless depending only on the ratio

dx.doi.org/10.1021/ma5006638 | Macromolecules 2014, 47, 3895−3900

(R/D). The scaling relation of eq 4 holds for an ideal chain confined in a slit, in a cylindrical pore, or in a hollow sphere with only a different coefficient.[44,45] However, in the present case the radius of gyration is much smaller than the smallest pore diameter. For example, in I_{74} (M_w = 5000 g/mol) R is 5.6 nm, the smallest pore diameter is 25 nm, and the contribution from confinement effects to the free energy is only $F_{conf}/k_BT \sim$ 5%. Hence, pure confinement effects have only a minor contribution and cannot explain the experimental findings.

A chain however can stick slightly to the pore walls forming larger loops that extend to an average distance of D. According to the de Gennes scaling formalism,[44] the free energy per chain is now given by

$$\frac{F_{total}}{k_BT} \cong \left(\frac{R}{D}\right)^2 - \delta f N \quad (5)$$

In eq 5, the first term is the confinement energy while the second term gives the interactions with the pore walls. In this term, $k_BT\delta$ gives the effective attraction of a monomer adsorbed at the surface and f is the fraction of adsorbed monomers. We should keep in mind that single chain adsorption is never realized in practice; the phenomenon is dynamic as many chains compete for the same portion of the surface.

The dielectric strength of the segmental and chain modes contains additional information that supports this picture. Figure 8 gives the normalized intensities of both chain and segmental modes for I_7 in the bulk and inside AAO with two pore diameters.

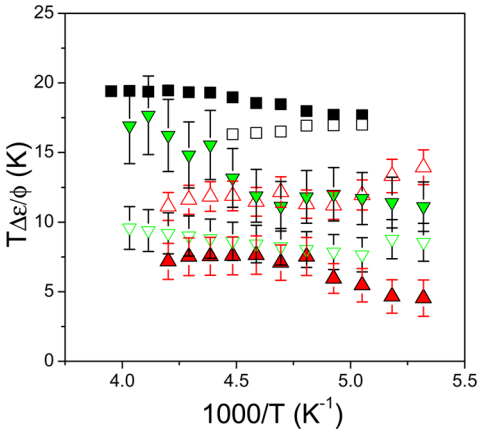

Figure 8. Dielectric relaxation strength of the chain (filled symbols) and segmental (open symbols) modes of I_7 normalized to the PI volume fraction (φ) within AAO: bulk I_7 (squares), I_7 located inside self-ordered AAO with pore diameters of 400 nm (up triangles), and 65 nm (down triangles).

It can be seen that both intensities are suppressed relevant to the bulk. For example, for I_7 within self-ordered AAO with pore diameter of 400 nm, the segmental mode intensity is reduced by 30%. This allows estimating the fraction of adsorbed monomers (f in eq 5). However, the uncertainty in the normalized intensities do not allow for a more quantitative comparison (i.e., as a function of pore size and as a function of polymer molecular weight).

Chain adsorption involves a wide range of time and length scales. Detailed knowledge of chain conformation including the distribution of different configuration building blocks (trains, loops, tails) as a function of the degree of adhesion is required. In this respect molecular dynamics simulations both at the atomistic and more coarse-grained models can shed light on the structural and dynamic properties of chains.[46] A mean-field-like lattice model was employed to obtain theoretical predictions for the size distribution of trains, loops, and tails.[46] A more recent coarse-grained bead−spring model studied the structure and dynamics of a polymer melt near attractive (or neutral) atomically smooth surfaces.[46] The study with respect to the statics revealed that (i) the number of loops, trains, and tails increase with increasing molecular weight, (ii) the length of trains is nearly independent of molecular weight whereas the length of tails increases linearly with molecular weight, and (iii) all these chain perturbations extend over a size R_g of polymer chains. With respect to the dynamics, a slower molecular mobility was found near the strongly attractive surface as compared to the bulk of the film.

The main experimental findings were the pronounced broadening of both segmental and chain modes with decreasing AAO pore diameter as well as the slower most intense chain dynamics for the lower molecular weights (I_4 and I_7). Furthermore, the broadening of the slower process suggests that the global chain relaxation is severely retarded on confinement. These findings can be discussed in the light of the MD simulations results. First, we estimate the number of monomers within a distance of R_g from the pore walls for different pore diameters. For I_{74} as an example, we find that the number of monomers varies from 2% (in AAO with a pore diameter of 400 nm) to 30% (in AAO with pore diameter of 25 nm). This suggests that within the smaller pores a large number of repeat units find themselves in configurations (trains, loops, tails) distinctly different from bulk conformations. This effect is more pronounced with increasing molecular weight as observed experimentally. Interestingly, DS is sensitive even to the smaller fraction of perturbed configurations within the AAO with pore diameter of 400 nm. Since both slopes, m and mn, are effected by the confinement, this may suggest that both inter- and intramolecular scale motions are influenced by adsorption.

This situation is shown schematically in Figure 9 for a given molecular weight in two different AAO nanopores. A fraction of chains with nonideal configurations exist within $2R_g$ from the pore walls and this fraction increase with decreasing pore diameter. For the lowest molecular weights, the whole chain can be a part of a train or a loop thus slowing down the chain

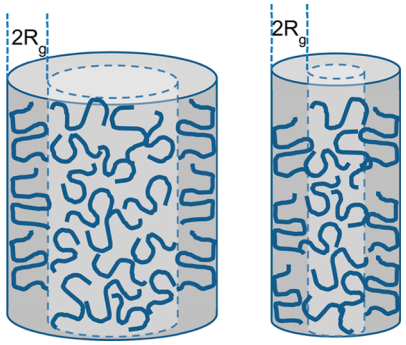

Figure 9. Schematic representation of chain conformations within pores with large and small diameters. Different chain configurations (trains, loops, tails) of adsorbed chains exist within $2R_g$ from the pore walls. The fraction of these configurations relative to the unperturbed chains is a strong function of pore diameter.

dx.doi.org/10.1021/ma5006638 | Macromolecules 2014, 47, 3895−3900

relaxation. In any case, the global chain relaxation is retarded on confinement.

IV. CONCLUSION

PI wets alumina and easily fills self-ordered AAO pores through the favorable attractive interactions with the pore walls. This facilitated a study of the effect of uniform 2D-confinement on the segmental and chain dynamics of the archetypal type A polymer (PI) as a function of molecular weight and pore size. The glass temperature was unaffected by confinement. However, a remarkable broadening of the distribution of relaxation times for both the segmental and chain modes was found even within pores with size 50 times the unperturbed chain dimensions. In addition, slower chain dynamics were found in the lower molecular weights. The pronounced broadening of the chain modes revealed that the global chain relaxation is severely retarded for PIs located inside self-ordered AAO. Confinement effects are negligible for the studied molecular weights. Chain adsorption, on the other hand, involves time and length scales distinctly different from the bulk that can account for the experimental findings.

■ ASSOCIATED CONTENT

Supporting Information

Figures S1 and S2. This material is available free of charge via the Internet at http://pubs.acs.org.

■ AUTHOR INFORMATION

Corresponding Author

*E-mail gfloudas@cc.uoi.gr (G.F.).

Notes

The authors declare no competing financial interest.

■ ACKNOWLEDGMENTS

The current work was supported by the Research unit on Dynamics and Thermodynamics of the UoI cofinanced by the European Union and the Greek state under NSRF 2007-2013 (Region of Epirus, call 18) and the operational program of the NSRF "Aristeia". M.S. gratefully acknowledges financial support from the German Research Foundation (STE 1127/9 and INST 190/134-1). Sample preparation by C. Hess and H. Tobergte as well as SEM investigations by G. Glasser and Y. Suzuki are gratefully acknowledged. We are also thankful to A. Milchev, V. G. Rostashvili, and T. A. Vilgis for helpful discussions.

■ REFERENCES

(1) Granick, S. *Science* **1991**, *253*, 1374.
(2) Shin, K.; Obukhov, S.; Chen, J.-T.; Huh, J.; Hwang, Y.; Mok, S.; Dobriyal, P.; Thiyagarajan, P.; Russell, T. P. *Nat. Mater.* **2007**, *6*, 961.
(3) Noirez, L.; Stillings, C.; Bardeau, J.-F.; Steinhart, M.; Schlitt, S.; Wendorff, J. H.; Pépy, G. *Macromolecules* **2013**, *46*, 4932.
(4) Scheutjens, J. M. K. M.; Fleer, G. J. *J. Phys. Chem.* **1980**, *84*, 178.
(5) Smith, G. D.; Yoon, D. Y.; Jaffe, R. L. *Macromolecules* **1992**, *25*, 7011.
(6) Schönhals, A.; Rittig, F.; Kärger, J. *J. Chem. Phys.* **2010**, *133*, 094903.
(7) Qi, D.; Fakhraai, Z.; Forrest, J. A. *Phys. Rev. Lett.* **2008**, *101*, 096101.
(8) Krutyeva, M.; Wischnewski, A.; Monkenbusch, M.; Willner, L.; Maiz, J.; Mijangos, C.; Arbe, A.; Colmenero, J.; Radulescu, A.; Holderer, O.; Ohl, M.; Richter, D. *Phys. Rev. Lett.* **2013**, *110*, 108303.
(9) Hofmann, M.; Hermann, A.; Ok, S.; Franz, C.; Kruk, D.; Saalwächter, K.; Steinhart, M.; Rössler, E. A. *Macromolecules* **2011**, *44*, 4017.
(10) Li, L.; Zhou, D.; Huang, D.; Xue, G. *Macromolecules* **2014**, *47*, 297.
(11) Petychakis, L.; Floudas, G.; Fleischer, G. *Europhys. Lett.* **1997**, *40*, 685.
(12) Jeon, S.; Granick, S. *Macromolecules* **2001**, *34*, 8490.
(13) Serghei, A.; Kremer, F. *Phys. Rev. Lett.* **2003**, *91*, 165702.
(14) Fukao, K. *Eur. Phys. J. E* **2003**, *12*, 119.
(15) Zhang, Q.; Archer, L. A. *Langmuir* **2003**, *19*, 8094.
(16) Elmahdy, M. M.; Chrissopoulou, K.; Afratis, A.; Floudas, G.; Anastasiadis, S. H. *Macromolecules* **2006**, *39*, 5170.
(17) Mapesa, E. U.; Tress, M.; Schulz, G.; Huth, H.; Schick, C.; Reiche, M.; Kremer, F. *Soft Matter* **2013**, *9*, 10592.
(18) Schönhals, A.; Goering, H.; Schick, Ch.; Frick, B.; Zorn, R. *Eur. Phys. J. E* **2003**, *12*, 173.
(19) Masuda, H.; Fukuda, K. *Science* **1995**, *268*, 1466.
(20) Masuda, H.; Hasegawa, F.; Ono, S. *J. Electrochem. Soc.* **1997**, *144*, L127.
(21) Masuda, H.; Yada, K.; Osaka, A. *Jpn. J. Appl. Phys.* **1998**, *37*, L1340.
(22) Steinhart, M. *Adv. Polym. Sci.* **2008**, *220*, 123.
(23) Hadjichristidis, N.; Iatrou, H.; Pispas, S.; Pitsikalis, M. *J. Polym. Sci., Part A: Polym. Chem.* **2000**, *38*, 3211. Uhrig, D.; Mays, J. W. *J. Polym. Sci., Part A: Polym. Chem.* **2005**, *43*, 6179.
(24) Kremer, F.; Schönhals, A. In *Broadband Dielectric Spectroscopy*; Springer: Berlin, 2002.
(25) Floudas, G.; Paluch, M.; Grzybowski, A.; Ngai, K. L. In *Molecular Dynamics of Glass-Forming Systems. Effects of Pressure*; Springer: Berlin, 2011.
(26) Floudas, G. Dielectric Spectroscopy. In *Polymer Science: A Comprehensive Reference*; Matyjaszewski, K., Möller, M., Eds.; Elsevier BV, Amsterdam, 2012; Vol. *2.32*, pp 825−845.
(27) Duran, H.; Gitsas, A.; Floudas, G.; Mondeshki, M.; Steinhart, M.; Knoll, W. *Macromolecules* **2009**, *42*, 2881.
(28) Havriliak, S.; Negami, S. *Polymer* **1967**, *8*, 161.
(29) Stockmayer, W. H. *Pure Appl. Chem.* **1967**, *15*, 539.
(30) Adachi, K.; Kotaka, T. *Macromolecules* **1985**, *18*, 466.
(31) Boese, D.; Kremer, F.; Fetters, J. *Macromolecules* **1990**, *23*, 1826.
(32) Yao, M.-L.; Watanabe, H.; Adachi, K.; Kotaka, T. *Macromolecules* **1991**, *24*, 6175.
(33) Schönhals, A. *Macromolecules* **1993**, *26*, 1309.
(34) Nicolai, T.; Floudas, G. *Macromolecules* **1998**, *31*, 2578.
(35) Floudas, G.; Meramveliotaki, K.; Hadjichristidis, N. *Macromolecules* **1999**, *32*, 7496.
(36) Floudas, G.; Reisinger, T. *J. Chem. Phys.* **1999**, *111*, 5201.
(37) Floudas, G.; Gravalides, C.; Reisinger, T.; Wegner, G. *J. Chem. Phys.* **1999**, *111*, 9847.
(38) Plazek, D. J.; Schlosser, E.; Schönhals, A.; Ngai, K. L. *J. Chem. Phys.* **1993**, *98*, 6488.
(39) Watanabe, H. *Macromol. Rapid Commun.* **2001**, *22*, 127.
(40) Kostov, K. S.; Freed, K. F.; Webb, E. B., III; Mondello, M.; Grest, G. S. *J. Chem. Phys.* **1998**, *108*, 9155.
(41) Theodorou, D. N. *Mol. Phys.* **2004**, *102*, 147.
(42) Fetters, L. J.; Lohse, D. J.; Richter, D.; Witten, T. A.; Zirkel, A. *Macromolecules* **1994**, *27*, 4639.
(43) Schönhals, A.; Schlosser, E. *Colloid Polym. Sci.* **1989**, *267*, 125.
(44) de Gennes, P.-G. *Scaling Concepts in Polymer Physics*; Cornell Univesrity Press: Ithaca, NY, 1979.
(45) Sakaue, T.; Raphaël, E. *Macromolecules* **2006**, *39*, 2621.
(46) De Virgiliis, A.; Milchev, A.; Rostiashvili, V. G.; Vilgis, T. A. *Eur. Phys. J. E* **2012**, *35*, 97.